Rheology of evolving bidisperse granular media

Raenell Soller, Jessica Cook, and Stephan A. Koehler

Phys. Rev. E **83**, 041305 — Published 26 April 2011

DOI: 10.1103/PhysRevE.83.041305

Rheology of evolving bidisperse granular media

Raenell Soller
Earth Science, Shorter University, Rome, GA 30165

Jessica Cook
Department of Physics, University of Massachusetts Amherst, MA 01003

Stephan A. Koehler
Department of Physics, WPI, Worcester, MA 01609 *

We investigate mixing of a bidisperse distributions of spherical particles for slowly rotating vanes by pouring smaller beads, diameter d_1, onto a monodisperse bed composed of larger beads, diameter d_0, and monitoring the torque and lift forces. If the mixing beads are too small, $d_1/d_0 < 0.05$, the drag and lift are unaltered. Otherwise smaller beads displace larger beads from the shearing region, and if present in sufficient quantity both the drag and lift diminish to values of a monodisperse bed composed entirely of the smaller beads. We observe reductions in the torque up to 70%. The rate at which smaller beads leave the shearing region decreases as their size relative to the larger beads increases, and for $d_1/d_0 > 0.155$ the smaller beads remain inside the shearing region.

PACS numbers: 45.70.-n,45.70.Mg,47.57.Gc,61.43.-j

* sak@wpi.edu

I. INTRODUCTION

Sheared granular materials display a rich, complex phenomenology, that in general remains poorly understood [1]. Several of these complex behaviors enter into our study shear mixing of bidisperse spherical particles. Shearing causes dilation [2], whereby the packing density decreases and pores expand [3, 4]. Large fluctuations occur, which in some cases abruptly transition to a jammed state [5–10]. Particle segregation has been studied in flows in hoppers and down inclined planes as well as rotating drums [11–16]. Vibrated granular beds exhibit fluid-like behavior, such as buoyancy [17], and size segregation. In certain situations the larger particles rise to the top of the bed which is known as the Brazil nut effect [18–21], whereas in others it is the smaller particles that rise to the top, which is known as the reverse Brazil nut effect [21, 22]. Since shearing leads to phase separation [23], rheological measurements of bidisperse granular mixtures are difficult because the granular material is evolving during the measurement. For these reasons most experiments are performed on media with a small degree of polydispersity or for small amounts of shear to minimize ordering effects [24], and consequently little is known about the rheology of polydisperse mixtures as they segregate.

Tardos et al. [25] performed granular rheology experiments on uniform granular media using a Couette geometry. They measured the torque, M, acting on a rotating cylinder, diameter D, partially immersed into a granular bed at depth z, and found that

$$M = \frac{c\nu\pi\rho g}{4} z^2 D^2 \ , \tag{1}$$

where ν is the packing density, ρ is the material density, and c is the frictional constant that for glass beads is $c \approx 0.5$. Based upon these results they developed a stress-strain model, which is proportional to the lithostatic pressure $p_{\rm litho} = \nu\rho g z$. Accordingly the shear stress is

$$\tau = c p_{\rm litho} \ . \tag{2}$$

Somewhat later Losert et al. [26, 27] performed similar Couette experiments, where they used imaging techniques to determine the radial dependence of the "granular temperature" from the jiggling of particles. They found that the root-mean-square fluctuations of the velocity had a power-law dependence on the rate of shear

$$V_{\rm RMS} \sim \dot{\gamma}^{0.4} \ , \tag{3}$$

and the width of the shear band is about ten particle diameters.

Soller and Koehler [28] also measured the torque of rotating geometries; however rather than using cylinders where issues of wall slip can be problematic, they chose parallelepiped vanes of width W and thickness T, see Fig. 1a. By defining a "vane diameter" $\mathcal{D} = \sqrt{T^2 + W^2}$, which is the diameter of the cylinder of rotation (see Fig. 1b), they found that the rotational drag was remarkably similar to that of Tardos' cylinders experiments, Eq. (1). However, they also found that the torque increases with particle size, which they included in a semi-empirical equation

$$M = c\nu\rho g \left(z + d/2\right)^2 \left(\mathcal{D} + d\right)^2 \ , \tag{4}$$

where $c \approx 0.6$ for glass beads [29]. Thus the vane's cylinder of rotation is augmented by a bead radius on the sides and the bottom, as is shown schematically in Fig. 1b. In addition they observed similar power-law behavior for the normal (lift) force on the rotating vane,

$$F = c^\star \nu\rho g \left(z + d/2\right)^{0.7} \left(\mathcal{D} + d\right)^{1.3} \ , \tag{5}$$

where $c^\star \approx 0.9$.

In a follow-up study, Soller and Koehler [10] observed that the fluctuations of the torque and lift also increase with the system granularity, which they defined as the ratio of the bead to vane diameter. They found the root-mean square strength of the fluctuations for the drag and lift approximately are

$$M_{\rm RMS} \approx 0.4 \frac{d}{\mathcal{D}} \ \text{ and } F_{\rm RMS} \approx 2 \frac{d}{\mathcal{D}} \ . \tag{6}$$

A few years later Daniel, Poloski and Sáez [30] performed rheological experiments using a four-blade vane *completely* submerged beneath the surface of the granular material consisting of fine glass beads. Their interpretation [31] is based upon an extension of the plane shearing models by DaCruz et al. [32] and Jop et al. [33]. Their resembles earlier models by Tardos et al. [25] and Soller et al. [28] in many respects, because it involves surface integrals over

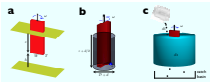

FIG. 1. a) Schematic of a parallelepiped vane with thickness T, width W, immersion depth z, and the height of the gap is h. b) The cylinder of rotation for estimating the torque is the vane diameter augmented by a particle diameter, $\mathcal{D} + d$, and the immersion depth augmented by a particle radius, $z + d/2$. c) Sketch of the mixing experiment with a sieve at the bottom: beads, diameter d_1, are poured into a monodisperse bed, diameter d_0, which drain, are collected and weighed in the catch basin below.

the cylinder of rotation for the lithostatic pressure, Eq. (2), and a friction coefficient(which they determined to be $c \approx 0.4$).

Segregation studies by Lominé and Oger [34, 35] examined the percolation of smaller particles, diameter d_1, draining through a static, dense granular bed of larger particles, diameter d_0. If they are sufficiently small, $d_1 \leq d_0/6.46$, the small beads poured onto a granular bed percolate through the bed similar to a pachinko gaming machine. The accumulation rate of the beads drained through the bed roughly follows a gaussian distribution which depends on bed height, concentration of the number of beads moving through the pores as well as other parameters, such as the aspect ratio and restitution coefficient. For low concentrations of percolating beads, the process is fairly well described by a convection-diffusion equation where the total mass of drained beads follows an error function

$$w \sim m \left[1 + \mathrm{erf}\left(\frac{k\,(t - t_0)}{\sqrt{2d_0/g}} \right) \right] , \tag{7}$$

where m is the mass of added particles, and the factor k as well as the delay time t_0 depends on d_1/d_0 and bed depth. As the flux of draining particles increases, they interfere with each other and the drainage process slows down. Thus the accumulation rate of w diminishes and diverges from Eq. (7). In fact it is possible for several smaller beads to get jammed and clog pores indefinitely as shown by Remond [36].

Surprisingly the rheology of bidisperse granular mixtures and their segregation dynamics has not been studied, despite the close link to mixing of different species using impellers in industrial settings. Our study focuses on the evolution of the rheology of a bidisperse granular mixture where the smaller species is poured onto a monodisperse granular bed and segregates during shearing. The shearing geometry is a slowly rotated vane, thus the media is in the quasi-static limit where inertial effects are minimal and the inertial number is small $I \ll 1$ [37]. We concluded that if the mixing particles fall within a certain size range they will displace the larger particles from the shearing region surrounding the vane, and if they are present in sufficient quantity inside the shearing region both the mean torque and its fluctuations approach values of a monodisperse bed composed entirely of mixing particles, cf. Eqs. (4) and (6). Depending on the size ratios the added beads drain through the bed or get clogged. If the particles are too small they will quickly drain through the granular bed without affecting the rheology.

II. METHODS

The mixing experiments are largely based upon earlier studies of parallelepiped vanes slowly rotated at angular velocity ω by an advanced rheometer (AR2000, TA Instruments) in monodisperse granular beds [10, 28]. The experiment begins with the vane partially immersed to depth z in a monodisperse bed of spherical particles diameter d_0, and has gap height, h, as shown in Fig. 1a. The gap height is defined as the distance between the vane's bottom surface and the bottom of the container. The resulting torque and lift (normal) force are measured as the bed approaches steady-state and the torque stabilizes at M_0. Next a certain mass, m_1, of mixing particles, diameter d_1, is quickly

poured by hand into the vortex generated by the vane's rotation, see Fig. 1b, which takes about one or two seconds and sets the time $t = 0$. The changing torque is monitored for an extended period of time (up to several hours) as the particles segregate and the bed's surface equilibrates, resulting in a final torque M_1 and immersion depth z_1. The third and final step is a slow withdrawal of the rotating vane out of the granular bed, where the torque diminishes to zero once the vane is completely withdrawn, which determines the immersion depth.

We performed two types of studies that required different containers with the rheometer's load cell performing different functions. In the first study a large dish, diameter about 20 cm, is placed on top of the load cell as in previous work [10, 28]. The rheometer's load cell monitors the vertical forces due to shearing and the weight of the added particles. The second container had a coarse sieve at its bottom, which allows smaller particles to drop out of the granular bed into a catch basin resting on the load cell, as shown in Fig. 1c. Here the load cell measures the accumulation of the drained particles.

In the study three types of particles were used:

1. $d = 0.2,\ 0.5,\ 0.9,\ 2,\ 5$ mm soda lime glass beads, material density $\rho = 2.55$ g/cm^3
2. $d = 6$ mm polystyrene pellets (intended for BB guns), material density $\rho = 1.02$ g/cm^3
3. $d = 2$ mm lead pellets (intended for BB guns), material density $\rho = 11.3$ g/cm^3.

After completion of the mixing experiments the beads were sifted by shaking in sieves and then reused.

We employed five different vane geometries with lateral dimensions $T \times W = 0.5 \times 6,\ 3.2 \times 12.7,\ 12.7 \times 25.4,\ 1.1 \times 38.1$ and 12.7×50.8 mm^2.

III. RESULTS AND DISCUSSION

Rather than separately presenting results and discussions in disjointed sections, we chose to combine the two into a single narrative for the sake of coherency. We begin with simple geometric considerations of how small particles pass through the pores of a granular bed and relate these to visual observations. The parameter space spans ten independent variables, $d_0,\ d_1,\ \rho_0,\ \rho_1,\ h,\ T,\ W,\ z_0,\ m_1$ and ω, all of which affect the dynamics of drag and lift. We present the most important and representative results of a large parametric study to provide a stream-lined description. We change the mass of the mixing particles, m_1, for the five different sizes of glass beads, d_1, and compare the torque with that for monodisperse beds in section § III B. We investigate how particle drainage (i.e. phase segregation) is affected by the gap height, h, in section § III C. In section § III D we present the dependence of mixing on the vane's angular velocity, ω. We examine the statistical variations of repeating mixing experiments in section § III E. Section § III F deals with changing the vane's immersion depth, and is followed by section § III G, where the vane size is varied. Finally, in section § III H we investigate the effects of changing the density of the mixing beads, ρ_1, relative to those of the monodisperse bed, ρ_0. Although the parameter space is considerable, we find a relatively straight-forward, unifying picture of mixing.

A. Geometric considerations and visual observations

We start with geometric considerations of the interstitial spaces inside a granular bed composed of monodisperse spheres, because these determine the motion of mixing particles. It is well-known that shearing leads to dilation [2], so in the shearing region a variety of local configurations will result that are looser than random packing. Recently several tomographic X-ray studies of static granular beds [38–40] have investigated local packing configurations for different volume fractions, and others have imaged particle rotation resulting from shear [41], but as far as we are aware there is no study of the pores in continuously sheared granular beds. We therefore give simple geometric arguments for how the mixing particles drain and get trapped in sheared beds and provide examples for our standard monodisperse bed, which has $d_0 = 5$ mm glass beads.

The smallest constriction in a monodisperse packing is the region bounded by three touching spheres, as shown in Fig. 2a and occurs in hexagonal close-packing (hcp), with particle fraction $\nu = 0.76$. This sets a limit on the largest sphere which can pass through the smallest constriction, which has diameter $\left(2/\sqrt{3} - 1\right) d_0 \approx 0.155 d_0$. Thus for the standard bed ($d_0 = 5$ mm), a necessary condition for particles to pass through the entire bed is $d_1 \leq 0.775$ mm. The smallest constriction for two identical neighboring spheres in contact with a wall, such as the side of the vane or container is shown in Fig. 2b. The largest sphere passing through this constriction has diameter $d_1/d_0 = 1/4$, which sets an upper bound of $d_1 \leq 1.25$ mm for the standard $d_0 = 5$ mm bed. Next we consider a maximally dilated planar configuration of four touching spheres which can result from shearing and whose cross-section is shown in Fig. 2c. The

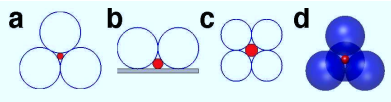

FIG. 2. The largest sphere that can fit inside the pores of different packing scenarios. a) The smallest constriction is in the plane of three touching spheres, and the largest enclosed circle has diameter $d_1 = \left(2/\sqrt{3} - 1\right) d_0 \approx 0.155 d_0$, b) Two touching spheres in contact with a wall, $d_1 = 1/4 d_0$, c) Four dilated, in-plane, touching spheres can accommodate a $d = \sqrt{2} - 1 \approx 0.414$ sphere in their middle. d) Four closely-packed spheres can accommodate a $d_1 = \left(\sqrt{3/2} - 1\right) d_0 \approx 0.225 d_0$ sphere at their center.

largest interior circle has diameter $(\sqrt{2} - 1)d_0$, which means that $d_1 \leq 2.07$ mm particles can pass through this pore in the standard bed. Finally, the largest sphere that can fit inside an hcp packing, shown in Fig. 2d, has diameter $(\sqrt{3/2} - 1)d_0 \approx 0.225 d_0$, which means that $d_1 \leq 1.12$ mm particles can be trapped inside the standard bed without causing expansion.

Visual observations of the mixing experiments show three distinct types of drainage behaviors, which are summarized in Fig. 3. These observations are corroborated by carefully removing layers of the mixture from the top and noting the composition of the bed as a function of vertical position. The $d_1 = 0.5$ mm beads are sufficiently small so they can pass through all constrictions, cf. Fig. 2a, and drain quickly through the granular bed to the bottom of the container. In sufficient quantity they will form a mound within the interstitial spaces of the coarser background bed which we call "bottom pile up", and is shown schematically in Fig. 3a. On the other hand, the $d_1 = 0.9$ mm particles cannot pass through dense regions, but can either pass through pores contacting the rotating vane or between dilated packings of four touching spheres as shown in Figs. 2b and 2c respectively. Away from the vane and the shear-dilated regions, these particles get trapped inside tetrahedral arrangements as shown in Fig. 2d. Thus 0.9 mm mixing beads cannot drain out of the bed, and instead accumulate in the region surrounding the rotating vane as is schematically represented in Fig. 3b. An additional type of behavior is "surface mounding", where a portion of the mixing particles remain in a mound as is illustrated in Fig. 3c. Here no pores are available for mixing beads at the surface, which may be because they are too big or all available pores are already saturated with mixing beads. Note that surface

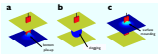

FIG. 3. Observations of different types of flow behaviors of the mixing particles where the bed's bottom and top free surface are schematically drawn. a) Small, $d_1 = 0.5$ mm beads quickly drain down and accumulate at the bottom of the dish. b) The $d_1 = 0.9$ mm beads remain in the vicinity of the rotating vane. c) Only a small amount of the $d_1 = 2$ mm beads drain, and the rest remains on the surface.

mounding can even occur for small beads, provided these are present in sufficient quantity such that the bottom pile-up mound extends to the top surface.

B. Increasing poured mass for different mixing bead sizes

In this section we discuss how the torque evolves during mixing for different masses, m_1, under standard conditions which are defined as $d_0 = 5$ mm, $T \times W = 12.7$ mm $\times$ 25.4 mm, $\omega = 2$ rad/sec, $z_0 = 30$ mm and gap height that is $h \approx 65$ mm.

Scenario **A**: Mixing beads with $d_1/d_0 = 0.1$. Fig. 4a shows the torque traces for five increasing mixing masses with $m_1 = 50,\ 75,\ 100,\ 200$ and 300 g and $d_1 = 0.5$ mm. The figure titles list the mixing mass m_1, as well as the initial and final immersion depths, z_0 and z_1 respectively. The black curves show the time-averaged torque, and the width of the cyan band in the background shows the extent of the RMS fluctuations. When the beads are poured into the monodisperse bed there is a spike in the torque, which sets the starting time of the experiment. The torque drops and reaches a minimum. For $m_1 \geq 100$ g the minimum is close to the value predicted by Eq. (4) using the mixing bead diameter d_1; this value is shown as horizontal dashed lines in Fig. 4a. The duration of the torque valley increases with m_1, and is characterized by the time T_M, where the torque remains below half of the plateau value. Note that the RMS noise in the valley is considerably smaller than at the beginning or end of the experiment, which is in agreement with the prediction of Eq. (6) where the mixing beads displace those of the monodisperse bed. Also, as discussed in section § III C, both the lift forces and their RMS noise diminishes when mixing beads are present in the shearing region.

Fig. 4b shows the torque as the vane is slowly withdrawn from the mixture. The dashed lines show the torques for withdrawal from monodisperse 0.5 mm and 5 mm beds. The withdrawal torques overlap those for a 5 mm bed, indicating that no mixing beads remain in the shearing region. Finally, the slow withdrawal measurements allow accurate determination of the final immersion depth, z_1, which is given in titles. The dashed vertical line indicates the initial immersion depth, which is typically a few mm greater than the final immersion depth.

This scenario involves five steps, which are are shown schematically in Fig. 5A:

i. pouring of mixing particles results in a heap on the bed and cause a spike in the torque.

ii. mixing particles descend into the shearing region below, displace the larger particles, surround the vane with smaller particles and thereby lower the torque and its RMS fluctuations. (Also the lift force is diminished, which is discussed below and shown in Fig. 8b.)

iii. mixing particles migrate out of the shearing region, and the torque (and lift) approaches its original level.

iv. mixing particles drain to the bottom of the bed.

v. the rotating vane is slowly withdrawn from a monodisperse bed composed entirely of large particles.

It is noteworthy that the relaxation time, T_M, is no greater than 100 sec for smaller masses $m_1 \leq 200$ g, but increases dramatically to about 300 sec for $m_1 = 300$ g. A possible explanation for this increase in relaxation time

is that bottom pile-up (cf. Fig. 3a) only becomes an issue for $m_1 > 200$ g. A simple estimate of the interstitial volume of a 45° cone with radius and height equal to the gap height, $h = 65$ mm, is 115 cm^3 which is filled by about 200 g of the smaller beads. Therefore greater amounts of mixing beads result in taller and wider cones which would partially contain the rotating geometry. Accordingly smaller particles remain inside the shearing region longer until they migrate out laterally or agitation reduces the height of the interstitial pile. In section § III C below we discuss how the use of a sieve prevents bottom pile-up and dramatically reduces the relaxation time to less than 100 sec for all values of m_1.

Scenario **B**: Small amounts of mixing beads with $0.18 \leq d_1/d_0 \leq 0.4$. Here mixing beads can only pass through dilated regions of the bed which are limited to the vicinity of the rotating vane. For small amounts of mixing beads the behavior is similar to Scenario **A** except that the mixing beads do not drain through the bed. The first two torque traces for $d_1 = 0.9$ mm with $m_1 = 50$ and 75 g in Fig. 6a show the initial spike due to pouring and a valley that approaches the horizontal dashed line which is the torque for a monodisperse bed composed of 0.9 mm beads where the vane is immersed to the same depth z_1. The subsequent withdrawals, shown in Fig. 6b, are the same as for a monodisperse 5 mm bed. Likewise, the first two traces for $d_1 = 2$ mm with $m_1 = 25$ and 50 g in Figs. 7a and 7b also exhibit this behavior.

Note that unlike Scenario **A**, here the bed height increases slightly (resulting in an equivalent increase of of the immersion depth, z_1, after pouring) which is evidenced by slightly longer withdrawals in Figs. 6b and 7b. These beads remain in the vicinity of the shearing region and their size causes the bed to expand upwards, where the expansion for the 2 mm beads is greater than for the 0.9 mm beads – see the end of section § III A.

This scenario involves four steps, shown in Fig. 5B, which are

i. pouring of mixing particles results in a heap on the bed and cause a spike in the torque.

ii. mixing particles descend into the shearing region below, displace the larger particles, surround the vane and thereby lower the torque and RMS fluctuations.

iii. mixing particles migrate out of the shearing region into the peripheral dilated regions, and the torque starts climbing towards its original level.

iv. the rotating vane is slowly withdrawn from the shearing volume, which at this point is composed almost entirely of the original large beads. (See the 50 and 75 g torque traces of Fig. 6b.)

Scenario **C**: Large amounts of mixing beads with $0.18 \leq d_1/d_0 \leq 0.4$. Unlike the previous scenario, the amount of mixing beads is sufficient to maintain saturation of the shearing region. This is the case for the last two torque traces of the $d_1 = 0.9$ and 2 mm torque traces of Figs. 6a and 7a. A portion of the mixing beads displace the larger beads from the shearing volume and saturate the dilated regions. The remaining beads contribute to an increased immersion depth z_1, as they are integrated into the 5 mm granular bed. Therefore, the dashed horizontal lines of Figs. 6a and 7a, which represent the torque for the smaller beads at the appropriate vane immersion depth, increase in value with the mass of mixing beads. Furthermore, the torque drops (e. g. Fig. 6a, 75 g) and torque withdrawals (Figs. 6b and 7b) are nearly the same as those for a monodisperse bed composed entirely of mixing beads of size d_1. This behavior is in contrast to the torque withdrawals for Scenario **B**, which follow a withdrawal for a bed composed entirely of beads of size d_0.

Although the torque does not drop significantly from its initial value after addition of mixing beads, it in fact is close to the predicted torque for a bed composed entirely of mixing beads using Eq. (4) for an increased immersion depth. Recall the immersion depth increases because a surface mound of mixing beads forms, which is evidenced by longer withdrawals. The withdrawals are up to 10 mm longer, indicating that the surface mound is about 10 mm tall. Therefore the dashed horizontal lines of Figs. 6a and 7a, which represent the torque for the smaller beads at the appropriate vane immersion depth, are increasing in value with the addition of mixing beads.

This scenario involves four steps, shown in Fig. 5C, which are

i. pouring of mixing particles results in a heap on the bed, and cause a spike in the torque.

ii. a portion of the mixing particles descends into the shearing region below, displaces the larger particles, surrounds the vane with smaller particles. The decrease in torque due to replacement by smaller particles is offset by a greater immersion depth due to surface mounding.

iii. as mixing particles migrate out of the shearing region into the peripheral dilated regions they are replaced by particles from the surface mound. Thus the torque drops slightly over time as the vane's immersion depth decreases.

iv. the rotating vane is slowly withdrawn from a region saturated with mixing beads.

Note that there are two mixing particle masses, $m_1 = 100$ g for $d_1 = 0.9$ mm and $m_1 = 75$ g for $d_1 = 2$ mm, where intermediate behavior is observed and results in a combination of Scenarios **A** and **B**. Although the torque during withdrawal starts off closer to the lower value for a bed composed of mixing beads, it switches over to the greater value for a bed composed of 5 mm beads. Thus the lower portion of the shearing region contains smaller beads; whereas, the upper portion of the shearing region contains larger beads. In these two experiments, the quantity of mixing beads is constrained to the periphery area and shearing region. The mass is not large enough to fill the shearing region, and hence the mixing beads have drained out of the top portion of the bed leaving only the 5 mm beads behind.

Scenario **D**: Small mixing beads with $d_1/d_0 = 0.04$. We also performed mixing experiments with $d_1 = 0.2$ mm glass beads, where the change in torque is so small that it is difficult to discern from the noise. These particles easily pass through any constriction, see Fig. 2a, and drain very quickly. It appears that they are too small to displace any of the larger beads from the vane's shearing region and affect the torque.

Scenario **E**: Addition of $d_1 = 5$ mm beads. Addition of these particles increases the torque, which only slightly decreases over time. The subsequent withdrawals are the same as those for a monodisperse 5 mm bed, where the immersion depth is greater than the initial immersion depth, which is due to a persistent surface mound that slowly erodes over time.

To summarize, we observe for $0.1 \leq d_1/d_0 \leq 0.4$ mixing beads that the minimum mass required for lowering the torque to values approaching those for monodisperse beds composed of mixing beads is about $m_1 \sim 100$ g. Assuming that indeed the shearing region is composed entirely of mixing beads, $m_1 \sim 100$ g corresponds to approximately a shearing region of about 10 diameters of the $d_0 = 5$ mm beads. This length scale has also been observed in Couette experiments [26]: the radial distance from the rotating cylinder over which the particle motion drops to zero is ten bead diameters. But visual observations show the composition of the vane's shearing region is a combination of small beads with some large ones, which possibly explains why the torque valley generally is above the equivalent torque of a bed composed entirely of the mixing beads.

C. Drainage out of the bed

Here we investigate the drainage process by which mixing particles exit the shearing region and move through the bulk. We discuss how this process is affected by the gap height, amount of mixing particles and container type (sieve or no sieve at the bottom).

Fig. 8a compares the dynamics of a sieve vs. a glass bottom experiment for $m_1 = 300$ g of $d_1 = 0.5$ mm beads. Particles leave the shearing zone about five times faster for the sieve; the recovery time is $T_M = 60$ rather than 300 sec. This is close to the recovery time for smaller masses $m_1 \leq 200$ g shown in Fig. 4a, because the sieve prevents bottom pile up that is the cause for the long relaxation time of the $m_1 = 300$ g glass bottom trial. For the sieve the lowest torque occurs at 33 sec, at which time 160 g of the mixing beads are still inside the bed.

Fig. 8b shows the normal force as registered by the load cell on which the glass dish is resting, and the width of the cyan band in the background shows its RMS noise. At $t = 0$ the normal force spikes due to the impact of the poured beads, and over time changes due to the changing lift force, which depends on the changing immersion depth and the beads surrounding the vane [28]. The normal force slowly drops for the first $t \sim 260$ sec, and starts to increase at about 100 sec after the torque has started increasing. The delay is to be expected considering that the beads drain downwards and the source of the normal force is the vane bottom; whereas, the source of the torque is the vane's sides. Similar to the torque the normal force levels off again at $t \sim 310$ sec. Also, the RMS noise of the normal force, indicated by the width of the cyan band, is lower in the valley as predicted by Eq. (6) for smaller beads.

Fig. 8c shows the weight of the mixing particles that have drained through the bed. At $t = 60$ sec the torque has recovered to its plateau value, and about 80% of the beads have passed through the sieve. The weight increases slowly over time towards $w \to 300$ g, and although these particles are small enough to pass through pores even after several minutes, several particles remain trapped inside (clogged) [36]. Agitation provided by the rotating vane slowly releases (unjams) some of the trapped particles. A rough estimate of the drainage speed of these particles is about 1 mm/sec, although some particles travel through the bed several times faster whereas others never make it out of the bed. Comparison with drainage experiments of Lomine and Oger [34] without shearing is difficult because different bead size ratios were used; however, shearing significantly accelerates the drainage rate (factor of five or more).

We further investigate particle drainage by examining how far particles of different sizes can drain through the bed and accumulate in the catch basin. We vary the gap height and determine the weight of the drained particles for all three bead sizes and different masses m_1 after extended shearing. As the gap height increases the number of clogged beads increases and fewer beads drain through the bed. Even a portion of the smallest beads, $d_1 = 0.2$ and 0.5 mm, gets trapped in the bed. The solid red line of Fig. 9a shows that for $d_1 = 0.5$ mm the fraction of drained beads, w/m_1, is close to unity and slowly decreases with increasing gap height. For the $d_1 = 0.9$ mm beads there is a dramatic decrease in the fraction of drained particles at $h \approx 18$ mm, which is compatible with the geometric argument

that these particles can only drain through dilated regions near or within the shearing region and the shearing region only extends a few bead layers below the vane. For the larger $d_1 = 2$ mm particles the drainage distance drops to 10 mm because these can only pass through extremely dilated regions in the immediate vicinity of the rotating vane, cf. Fig. 2c.

D. Changing angular velocity

We performed a series of $d_1 = 0.9$ mm, $m_1 = 100$ g experiments for four angular velocities $\omega = 0.5,\ 2,\ 8$ and 32 rad/sec with a sieve bottom. Increasing the shearing rate speeds up the dynamics, which is shown in terms of the recovery times of the torque and drained weight, $T_M,\ T_w$ in Fig. 9b. Similar to the torque's recovery time, the recovery time of the drained weight, T_w, is defined as the duration for half of the particles to drain out of the container, see the dashed lines of Fig. 8c. The dashed triangle shows simple power-law behavior, $T_M,\ T_w \propto \omega^{-1/2}$, which captures the trends of the recovery times for $\omega < 32$ rad/sec. To validate this relationship, further studies are required that include varying the mass and size of the mixing beads, as well as immersion depth and vane height. It is intuitively clear that faster shearing leads to greater increased agitation, which results in faster drainage of the smaller particles. Dimensional analysis provides some insight. The two relevant time scales are due to shearing and gravity, $1/\omega$ and $\sqrt{d/g}$, and both must appear in the recovery time. Their geometric mean is $\omega^{-1/2} d^{1/4} g^{-1/4}$. A more rigorous explanation involves the root-mean-square velocities of the large beads, whose dependence on the shearing rate is given by Eq. (3). The rate at which the mixing particles can pass through pores is proportional to the agitation of the large beads, and thus

$$T_w \sim V_{\mathrm{RMS}}^{-1} \sim \dot{\gamma}^{-0.4} \sim \omega^{-0.4} \ . \tag{8}$$

This scaling prediction is in agreement with our measurements.

E. Variations in the dynamics

Even though pouring of mixing beads was done in a consistent manner there are substantial variations from trial to trial which are attributable to fluctuations inherent in granular systems. Fig. 10a shows a large variation in the recovery times of the torque $T_M = 1000 \pm 500$ sec among nine trials involving $m_1 = 100$ g and $d_1 = 0.5$ mm beads. On the other hand, the relative variation of the torque valley minimum is far less, $M_{\mathrm{valley}} = 1.55 \pm 0.1$ Ncm. Close inspection reveals that longer torque valleys generally are also deeper, which is consistent with the picture of clogged mixing particles; for situations where the clogging is more effective a larger portion of the mixing beads remain trapped inside the shearing region for longer periods of time.

Fig. 10b shows that similar to the torque, the dynamics of the drained particles fluctuates widely; the range is $400 \leq T_w/\mathrm{sec} \leq 2000$. Fig. 10c is a parametric plot of the torque and drained particle weight, which correlates the drainage and torque dynamics. The minimum of the torque valley occurs only when a small amount of mixing beds have passed, $5 \lesssim w/\mathrm{g} \lesssim 30$, which means that about 80 g of mixing particles inside the bed are needed to reduce the torque. This quantity compares well with similar mixing experiments shown in Fig. 6, where a substantial torque valley appears for $m_1 \gtrsim 75$ g.

F. Changing immersion depth

Here we discuss the effects of varying immersion depth on mixing dynamics. The immersion depth exceeds the vane diameter, $z > \mathcal{D}$, so we expect that relative drops in torque are primarily due to augmentation of the vane diameter, $\sim 2\,(d_1 - d_0)\,/\,(\mathcal{D} + d_0)$, provided sufficient mixing beads are present to saturate the shearing region.

Fig. 11 shows the torque traces for a series of $m_1 = 250$ g, $d_1 = 0.5$ mm mixing experiments at five different immersion depths varying from $z = 18$ to $z = 54$ mm. These show the same dynamics as Scenario **A** observed earlier. The torque traces exhibit a clear valley, whose minimum approaches the dashed line that represents the torque at depth z_1 in a $d_m = 0.5$ mm monodisperse bed within 10% or less.

The recovery times T_M generally increase with increasing immersion depth, although the fluctuations between trials are large and somewhat obscure this trend. The mass is sufficient for bottom pile-up of the small beads in the interstitial spaces extending up to the shearing region (cf. $m_1 = 200$ and 300 g in Fig. 4). A layer-by-layer removal of the beads after the experiment was completed. Thus with increasing immersion depth the vane is deeper inside the internal mound of 0.5 mm beads residing inside the interstitial spaces of the bed, which results in longer times for the particles to drain out of the shearing region.

G. Changing vane size

So far all experiments were performed with the standard vane, $T \times W = 12.7$ mm $\times$ 25.4 mm, and here we discuss results for changing the vane size. According to Eq. (4) we expect the greatest relative torque decrease for the smallest vanes (i.e. smallest values of $\mathcal{D}$) and smallest particles (provided they can displace the larger particles). Conversely, we expect to see the smallest change in torque for vanes that are large compared with the mixing beads.

Fig. 12 shows torque traces for four different vanes with $d_1 = 0.5$ mm mixing particles, ranging in diameter from $\mathcal{D} \approx 1.2d_0$ to $\mathcal{D} \approx 11d_0$. Fig. 12a shows that for the smallest vane the torque drop is a dramatic 70%! The minimum torque is close to that for a $d_m = 0.5$ mm bed as indicated by the dashed line. Note that this system is very granular, and hence abrupt changes in torque can result from re-arrangements only involving a few $d_0 = 5$ mm particles. For larger vanes, see Figs. 12b-d, the drop is less dramatic and the minimum torque is within 25% of the dashed lines. The torque in all cases returns to its original value, as expected for Scenario **A**. Additionally, the RMS fluctuations, indicated by the width of the cyan band, are smaller in the valleys (cf. Eq. (6)).

H. Changing bead density

Here we investigate the effects of varying the density of mixing beads. The standard vane is used, $T \times W =$ 12.7 mm $\times$ 25.4 mm, $\omega = 2$ rad/sec, $z_0 \approx 50$ mm and the bed is sufficiently deep so that bottom pile-up does not affect the measurements. However, in these experiments the monodisperse bed is composed of the lightest beads, which are $d_0 = 6$ mm polystyrene BBs, and the mixing particles are the heaviest, which are $d_1 = 2$ mm lead spherical BBs. Based upon the glass bead experiments above, one would expect to observe Scenarios **B** or **C** depending on how much has been added; however, the large difference in density has to be accounted for, and it is reasonable to expect that the resulting torques would substantially increase since the density of lead is over ten times that of plastic.

Fig. 13a shows torque traces for different mixing masses, $m_1 = 100,\ 200,\ 300$ and 500 g of 2 mm lead particles. The torque initially is $M_0 \approx 0.9 \pm 0.1$ Ncm, spikes to over 1.5 Ncm and settles down to values between 0.8 to 1.3 Ncm. Even for long periods of shear the torque slowly diminishes and never exhibits the decrease and subsequent increase as was observed for the glass bead experiments above. The subsequent withdrawals in Fig. 13b show that for larger amounts of mixing masses the torques start off above those for a monodisperse bed of plastic beads and after about 10 mm of withdrawal fall onto the curve for a monodisperse bed of 6 mm plastic beads. These withdrawals therefore are similar to those for $d_1 = 2$ mm glass beads with $m_1 < 100$ g shown in Fig. 7b, except that the torque approaches steady-state from above rather than below. But the lead beads are much denser, and so the reduction due to size, which diminishes the torque, is offset by the increase due to density, which increases the torque, see Eq. (4). In fact, one would naively expect the torque to increase tenfold when the lead BBs have saturated the shearing region, rather than the observed 10–20% increases. A possible explanation for the small increase in torque follows from considering the lithostatic pressure acting on the vane. The drag and lift forces are proportional to the lithostatic pressure, which is modified by the mixing beads. Since the region of the lead particles surrounding the vane is thin, varying from N=2 to 10 layers for the four different mixing masses, the lithostatic pressure does not increase to that of a bed composed entirely of lead BBs and instead remains closer to that of plastic BBs. Thus the resulting frictional forces on the vane are closer to those of $d_m = 2$ mm beads whose density is closer to that of plastic rather than lead.

Now we return to the torque traces of Fig. 13a. If indeed the lead particles move out of the shearing region into the peripheral regions as expected for Scenario **B**, then it may be puzzling that the torque does not return to its initial value, as is the case for the glass bead experiments, and instead stays elevated. The cause is an increase in the lithostatic pressure: lead particles in the peripheral region will elevate the lithostatic pressure of the shearing region and cause an increase in the torque.

IV. CONCLUSIONS

We have performed numerous mixing experiments of bidisperse granular media spanning a wide range of parameter space, and found a coherent simple picture regarding the dynamics of drag and lift on a slowly rotating vane as well as drainage of the mixing particles. If the mixing particles are much smaller than the smallest constriction in a granular bed, $d_1/d_0 \lesssim 0.05$, they will quickly flow through the bed with little affect. If their size is in the range $0.1 \lesssim d_1/d_0 < 0.5$, the mixing particles will displace larger ones and the greatest reduction in drag and lift occurs when a mass of mixing beads equivalent to ten or more layers of the larger particles have been displaced. The forces approach those of the vane rotating in a monodisperse bed composed of the smaller species. The dynamics follow three behaviors which depend on the relative size of the mixing beads. Smaller mixing particles, $d_1/d_0 \approx 0.1$, fit through all the pores but still are prone to clogging which extends the duration they remain in the shearing region.

Larger mixing particles, $0.18 \leq d_1/d_0 \leq 0.4$, can only move through dilated regions and therefore are confined to the vicinity of the rotating vane. Consequently the forces only recover to their original values if small amounts are added and otherwise do not change. If the density of the mixing beads is different, the forces are only affected somewhat and are far below the values for a monodisperse bed composed entirely of the denser mixing beads.

Direct visualization of the particles would be very useful in confirming this picture. In particular it would be helpful to determine how the mixing bead concentration varies over time. We hypothesize that during mixing the shearing contains some nontrivial fraction of larger beads. We propose the mechanism responsible for the decrease in torque and lift forces is due to a decrease in the effective vane diameter. However another mechanism may be responsible for the reduction in the torque and lift force, such as a ball-bearing type effect where the smaller beads act as ball bearings to facilitate rotation of the larger beads in the shearing region and reduce the amount of frustration [42].

ACKNOWLEDGMENTS

We thank Carlos Santamarina for stimulating discussions, and the comments of an anonymous referee. We acknowledge support from National Science Foundation grant # CTS-0626191215.

[1] G. MiDi, European Physical Journal E **14**, 341 (2004).
[2] O. Reynolds, Philosophical Magazine And Journal of Science, Fifth Series **50**, 469 (1885).
[3] H. Makse, D. Johnson, and L. M. Schwartz, Physical Review Letters **84**, 4160 (2000).
[4] Y. Forterre and O. Pouliquen, Annual Review of Fluid Mechanics **40**, 1 (2008).
[5] A. J. Liu and S. R. Nagel, Nature **396**, 21 (1998).
[6] I. Albert, P. Tegzes, B. Kahng, R. Albert, J. G. Sample, M. Pfeifer, A. L. Barabasi, T. Vicsek, and P. Schiffer, Physical Review Letters **84**, 5122 (2000).
[7] E. Longhi, N. Easwar, and N. Menon, Phys. Rev. Lett. **89**, 045501 (Jul 2002).
[8] C. S. O'Hern, L. E. Silbert, A. J. Liu, and S. R. Nagel, Physical Review E **68**, 011306 (2003).
[9] E. I. Corwin, H. M. Jaeger, and S. R. Nagel, Nature **435**, 1075 (2005).
[10] R. Soller and S. A. Koehler, Europhysics Letters **80**, 14004 (2007).
[11] A. Samadani, A. Pradhan, and A. Kudrolli, Phys. Rev. E **60**, 7203 (Dec 1999).
[12] S. Pudasaini and J. Mohring, Granular Matter **4**, 45 (JUL 2002).
[13] G. Félix and N. Thomas, Physical Review E **70** (NOV 2004).
[14] C. Goujon, B. Dalloz-Dubrujeaud, and N. Thomas, European Physical Journal E **23**, 199 (JUN 2007).
[15] P. G. Rognon, J.-N. Roux, M. Naaim, and F. Chevoir, Physics of Fluids **19** (MAY 2007).
[16] W. R. Ketterhagen, J. S. Curtis, C. R. Wassgren, and B. C. Hancock, Powder Technology **179**, 126 (JAN 1 2008).
[17] D. A. Huerta, V. Sosa, M. C. Vargas, and J. C. Ruiz-Suárez, Phys. Rev. E **72**, 031307 (Sep 2005).
[18] M. Alam, L. Trujillo, and H. J. Herrmann, Journal of Statistical Physics **124**, 587 (Aug 2006), ISSN 0022-4715.
[19] M. E. Mobius, B. E. Lauderdale, S. R. Nagel, and H. M. Jaeger, Nature **414**, 270 (2001).
[20] A. Rosato, K. J. Strandburg, F. Prinz, and R. H. Swendsen, Physical Review Letters **58**, 1038 (MAR 9 1987).
[21] M. Schröter, S. Ulrich, J. Kreft, J. B. Swift, and H. L. Swinney, Physical Review E **74**, 011307 (Jul 2006).
[22] T. Shinbrot and F. J. Muzzio, Phys. Rev. Lett. **81**, 4365 (Nov 1998).
[23] H. Herrmann and S. Luding, Continuum Mechanics and Thermodynamics **10**, 189 (AUG 1998).
[24] J. C. Tsai, G. A. Voth, and J. P. Gollub, Physical Review Letters **91**, 064301 (2003).
[25] G. I. Tardos, M. I. Khan, and D. G. Schaeffer, Physics of Fluids **10**, 335 (1998).
[26] W. Losert, L. Bocquet, T. C. Lubensky, and J. P. Gollub, Physical Review Letters **85**, 1428 (2000).
[27] L. Bocquet, W. Losert, D. Schalk, T. C. Lubensky, and J. P. Gollub, Physical Review E **65**, 011307 (2001).
[28] R. Soller and S. A. Koehler, Physical Review E **74**, 021305: 1 (2006).
[29] Compared with Tardos' results, we found the torque on the vane is about 60% greater than on the cylinder for glass beads.
[30] R. C. Daniel, A. P. Poloski, and A. E. Sáez, Powder Technology **191**, 237 (2008).
[31] R. C. Daniel, A. P. Poloski, and A. E. Sáez, Chemical Engineering Science **62**, 1343 (2007).
[32] F. da Cruz, S. Emam, M. Prochnow, J. N. Roux, and F. Chevoir, Physical Review E **72** (2005).
[33] P. Jop, Y. Forterre, and O. Pouliquen, Nature **441**, 727 (2006).
[34] F. Lomine and L. Oger, Journal of Statistical Mechanics - Theory and Experiment(JUL 2006).
[35] F. Lomine and L. Oger, Physical Review E **79** (MAY 2009).
[36] S. Remond, Physica A **309**, 4485 (2010).
[37] O. Pouliquen, C. Cassar, P. Jop, Y. Forterre, and M. Nicolas, Journal of Statistical Mechanics: Theory and Experiment **2006**, 14 (2006).
[38] G. T. Seidler, G. Martinez, L. H. Seeley, K. H. Kim, E. A. Behne, S. Zaranek, B. D. Chapman, S. M. Heald, and D. L. Brewe, Phys. Rev. E **62**, 8175 (Dec 2000).
[39] T. Aste, M. Saadatfar, and T. J. Senden, Physical Review E **71**, 061302 (2005).

[40] T. Aste, M. Saadatfar, and T. J. Senden, Journal of Statistical Mechanics: Theory and Experiment **2006**, P07010 (JUL 2006).
[41] K. A. Alshibli and B. A. Alramah, Journal of Geotechnical and Geoenvironmental Engineering **132**, 80 (2006).
[42] F. Alonso-Marroquín, I. Vardoulakis, H. J. Herrmann, D. Weatherley, and P. Mora, Phys. Rev. E **74**, 031306 (Sep 2006).

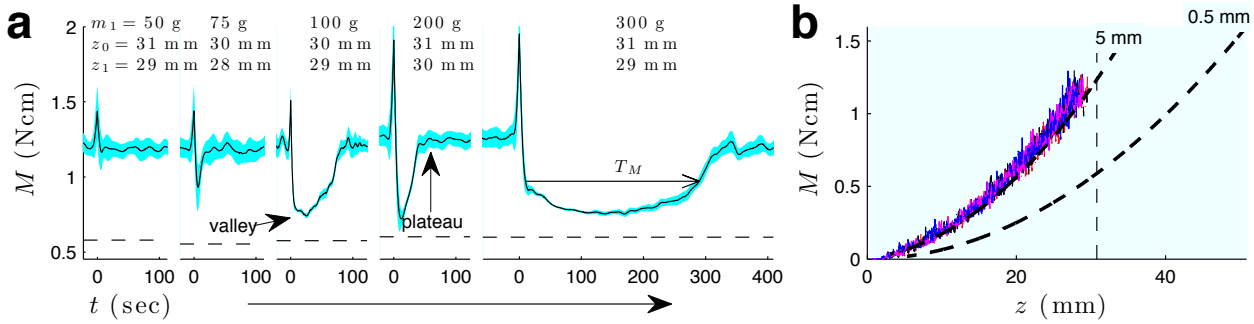

FIG. 4. a) Torque traces for increasing mass, m_1, of $d_1 = 0.5$ mm beads for standard conditions. The figure titles list the mixing mass m_1, as well as the initial and final immersion depths, z_0 and z_1 respectively. The dashed lines at the bottom show the equivalent torque for the vane immersed to depth z_1 into a $d_m = 0.5$ mm monodisperse bed. For the last $m_1 = 300$ g trace the arrow indicates the time T_M during which the torque is beneath half that of the plateau value. b) Dependence of the torque on the immersion depth during slow withdrawal. The dashed vertical line shows the initial immersion depth.

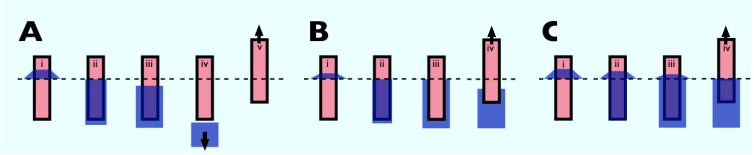

FIG. 5. Cartoons of the drainage process for standard conditions as described in the text. A) Mixing beads $d_1/d_0 \approx 0.1$. B) Small amounts of mixing beads with $0.18 \leq d_1/d_0 \leq 0.4$. C) Large amounts of mixing beads with $0.18 \leq d_1/d_0 \leq 0.4$.

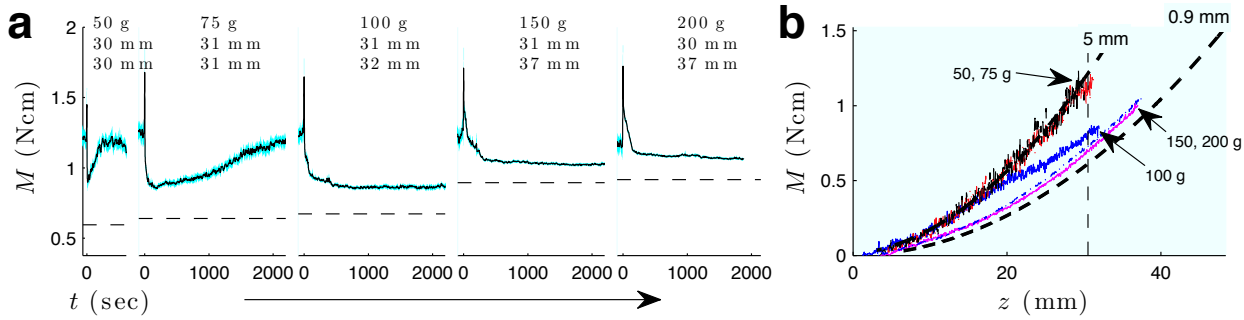

FIG. 6. a) Torque traces for increasing mass, m_1, of $d_1 = 0.9$ mm beads for standard conditions. b) Dependence of the torque on the immersion depth during slow withdrawal.

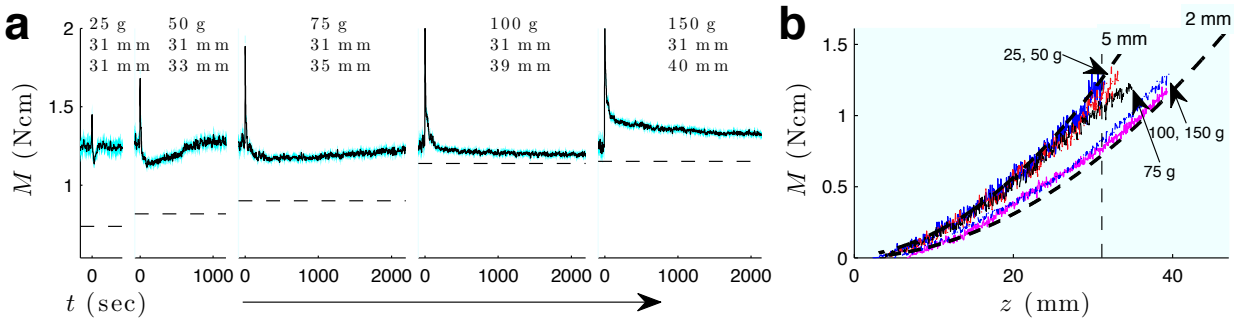

FIG. 7. a) Torque traces for increasing mass, m_1, of $d_1 = 2$ mm beads for standard conditions. b) Dependence of the torque on the immersion depth during slow withdrawal.

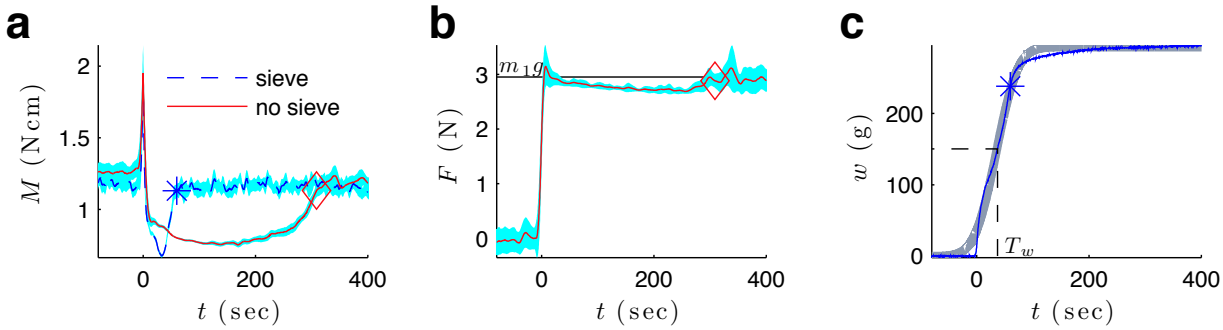

FIG. 8. a) Torque traces with and without a sieve for $m_1 = 300$ g and $d_1 = 0.5$ mm, where the gap heights are $h = 52$ and 95 mm respectively. The star, "⋆", and diamond, "⋄", indicate the times when the torque has returned to its plateau value with and without a sieve. b) Normal force for the glass dish, where the diamond shows that the normal force attains its plateau at the same time as the torque. The solid line in the background shows the weight of the added mass $m_1 g = 2.96$ N. c) Weight of the beads that have drained through the sieve. The time required for half the particles to drain out is $T_w = 37$ sec. The star shows that 80% of the beads have drained when the torque has returned to its plateau value. The thick gray curve in the background is the best fit to the error function Eq. (7).

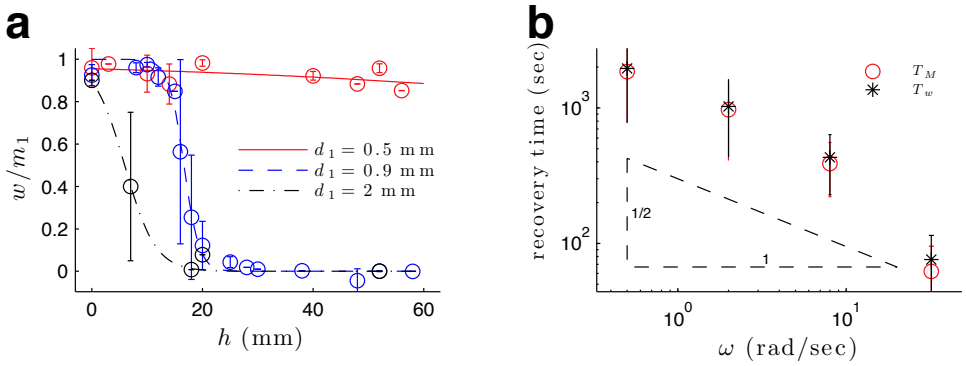

FIG. 9. a) The fraction of the drained mixing particles for different gap heights. The curves serve to guide the eye. b) Recovery times for the torque and drained weight for $m_1 = 100$ g, $d_1 = 0.9$ mm particles at $h = 12$ mm and immersion depth $z \approx 40$ mm. The error bars indicate the standard deviations from repeating the experiments nine times.

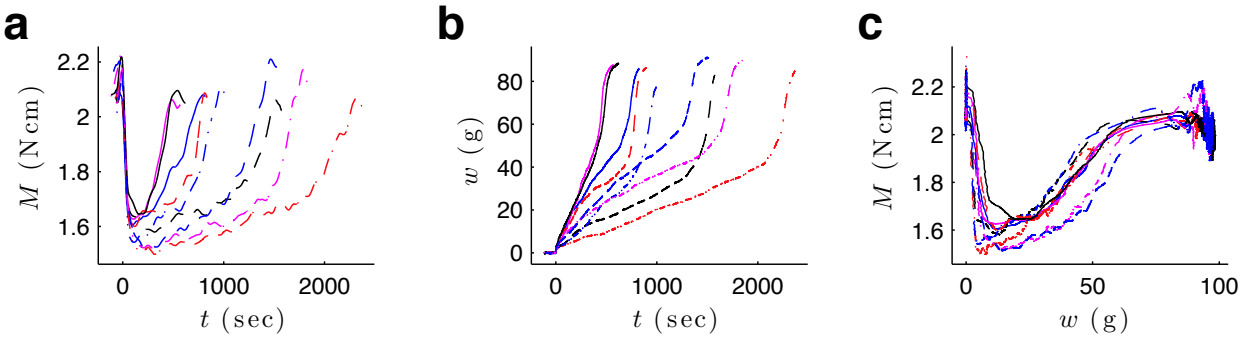

FIG. 10. Variations for 9 repeats using a sieve bottom with $d_1 = 0.9$ mm, $m_1 = 100$ g, $z \approx 40$ mm and $h = 12$ mm. Temporal evolution of a) the torque and b) the weight of the beads that have drained out. c) A parametric plot of the torque and drained weight.

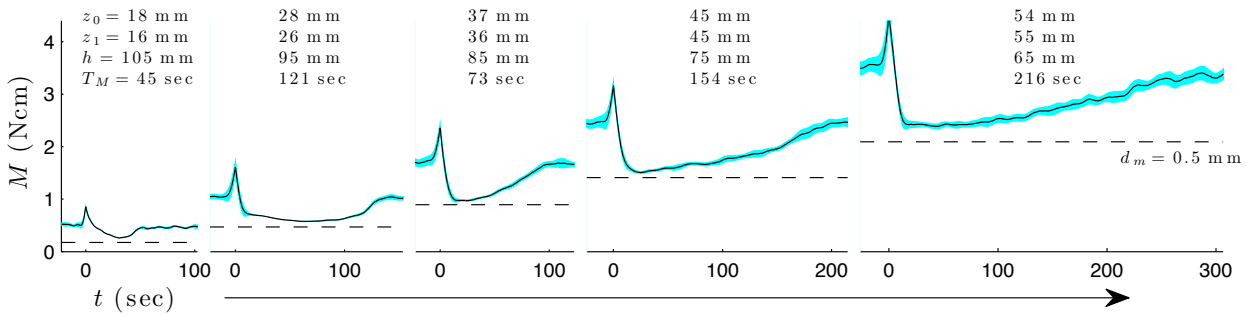

FIG. 11. Torque traces for $d_1 = 0.5$ mm and $m_1 = 250$ g and increasing initial immersion depths, $z_0 = 18,\ 28,\ 37,\ 45,\ 54$ mm. The dashed lines show the torques for an equivalent 0.5 mm monodisperse bed using the final immersion depth, z_1.

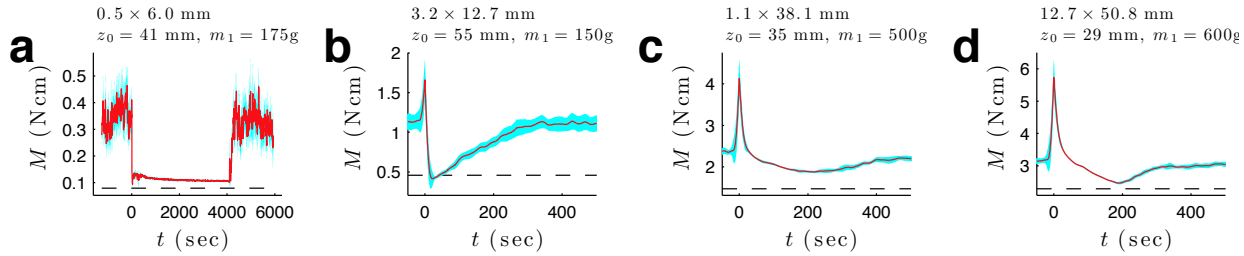

FIG. 12. Different vane geometries with $d_1 = 0.5$ mm mixing beads in a $d_0 = 5$ mm bed and $\omega = 2$ rad/sec. The dashed lines show the torque for a monodisperse 0.5 mm bed with the vane immersed to depth z_0.

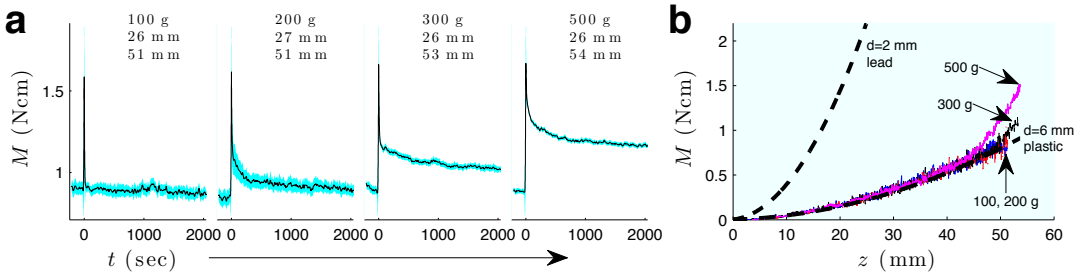

FIG. 13. Pouring $d_1 = 2$ mm lead beads, mass $m_1 = 100,\ 200, \ldots, 500$ g, into a $d_0 = 6$ polystyrene bed using the standard vane immersed to $z_0 = 46$ mm. a) Torque traces and the text gives both m_1 and z_1. b) Torque during withdrawal. The dashed curves show the torques for withdrawal from $d_m = 6$ mm polystyrene bead and $d_m = 2$ mm lead beads. The vertical dashed line shows the initial immersion depth.